Computer Physics Communications 188 (2015) 131–139

Contents lists available at ScienceDirect

Computer Physics Communications

journal homepage: www.elsevier.com/locate/cpc

Stabilized finite element methods to simulate the conductances of ion channels

Bin Tu [1], Yan Xie [1], Linbo Zhang, Benzhuo Lu *

State Key Laboratory of Scientific and Engineering Computing, Institute of Computational Mathematics and Scientific/Engineering Computing, Academy of Mathematics and Systems Science, Chinese Academy of Sciences, Beijing 100190, China

ARTICLE INFO

Article history:
Received 31 March 2014
Received in revised form
8 November 2014
Accepted 22 November 2014
Available online 3 December 2014

Keywords:
Ion channels
Poisson–Nernst–Planck equations
Stabilized finite element method
PRFB
SUPG

ABSTRACT

We have previously developed a finite element simulator, ichannel, to simulate ion transport through three-dimensional ion channel systems via solving the Poisson–Nernst–Planck equations (PNP) and Size-modified Poisson–Nernst–Planck equations (SMPNP), and succeeded in simulating some ion channel systems. However, the iterative solution between the coupled Poisson equation and the Nernst–Planck equations has difficulty converging for some large systems. One reason we found is that the NP equations are advection-dominated diffusion equations, which causes troubles in the usual FE solution. The stabilized schemes have been applied to compute fluids flow in various research fields. However, they have not been studied in the simulation of ion transport through three-dimensional models based on experimentally determined ion channel structures. In this paper, two stabilized techniques, the SUPG and the Pseudo Residual-Free Bubble function (PRFB) are introduced to enhance the numerical robustness and convergence performance of the finite element algorithm in ichannel. The conductances of the voltage dependent anion channel (VDAC) and the anthrax toxin protective antigen pore (PA) are simulated to validate the stabilization techniques. Those two stabilized schemes give reasonable results for the two proteins, with decent agreement with both experimental data and Brownian dynamics (BD) simulations. For a variety of numerical tests, it is found that the simulator effectively avoids previous numerical instability after introducing the stabilization methods. Comparison based on our test data set between the two stabilized schemes indicates both SUPG and PRFB have similar performance (the latter is slightly more accurate and stable), while SUPG is relatively more convenient to implement.

1. Introduction

Ion channels are essential for the proper function of cells and organisms [1]. Theoretical treatments of ion transport through channel proteins may be broadly classified as kinetic models, electrodiffusion models, and statistical mechanics based discrete model. The most commonly used theoretical techniques in the field are stochastic models, molecular dynamics (MD) [2] and Brownian dynamics (BD) [3–5]. Classical MD utilizes empirical interaction potentials or force fields calibrated by macroscopic data to describe molecular motions and is able to handle an entire ion channel, including ions, counterions, solvent, lipids and proteins. Unfortunately, there are two issues for commonly used MD methods: one issue is to develop appropriate force fields for the ionic mixtures and concentrated solutions in and near channels; the other issue is that, with MD, it is computationally costly and, in some situations, infeasible to reach the time scale of ion permeation across most channel membranes and to determine ion conductance. Compared to Brownian dynamics (BD) and molecular dynamics (MD), the continuum models, usually using a coarse approximation of continuum dielectric media and a static representation of proteins, have advantages of reducing computational cost and the ease of applying certain boundary conditions. A widely used electrodiffusion model is based on the Poisson–Nernst–Planck equations [6,7], in which ions are not treated as microscopic discrete entities but as continuous charge densities. Therefore, the PNP theory describes both the solvent and ions as continuous distributions. Consequently, there are limitations associated with the PNP model. It is well-known that the PNP theory neglects the finite volume effect of ion particles. Moreover, non-electrostatic interactions between ions are not accounted in the PNP model. PNP theory has previously been applied

* Corresponding author.
E-mail addresses: tubin@lsec.cc.ac.cn (B. Tu), xieyan@lsec.cc.ac.cn (Y. Xie), zlb@lsec.cc.ac.cn (L. Zhang), bzlu@lsec.cc.ac.cn (B.Z. Lu).
[1] Co-first authors.

http://dx.doi.org/10.1016/j.cpc.2014.11.018
0010-4655/

to the study of ion transport in electrochemical liquid junction systems [8] and electron transport in semiconductor devices [9], as well as ion permeation through biological membrane channels [10–12]. A number of numerical algorithms, including finite difference [13–16], finite element [17–19,12,20], spectral element [21] and finite volume methods [22], have been utilized in the past two decades for solving the PNP equations. Although the finite difference (FD) method is straightforward to implement, applying this method to systems that have curved boundaries and complicated geometries is challenging. If the surface and volume mesh of proteins are available, the finite element method has the advantage of naturally handling complex geometries, such as the molecular surfaces of DNA molecules and ion channels. Moreover, the finite element method has a solid mathematical foundation, and there are numerous user-friendly and mature FE software packages available for usage. We recently published one of the first works using FEM to solve the 3D PNP equations for ion channel systems [12]. However, there are still numerical challenges for solving PNP equations for simulating ion transport through large ion channel systems. In [12], we found some existing difficulties to simulate the biggest ion channel listed in the article [23]. Our recent analysis and studies indicate that if there is a strong electrostatic potential (which usually occurs in biomolecular systems), the NP equations have a large drift term (advection-dominated), which may result in numerical divergence with the standard finite element method.

In this paper, stabilized finite element methods are introduced to enhance the robustness of the solver. Stabilized finite element methods are formed by adding variational terms into the standard Galerkin method, which are mesh-dependent, consistent and numerically stabilizing. The Streamline-Upwind/Petrov–Galerkin (SUPG) method, introduced by Brooks and Hughes for advection–diffusion equations and incompressible Navier–Stokes equations [24], can be considered as the first successful stabilization technique to prevent oscillations in advection-dominated problems in the FEM. The main steps are as follows: (1) introduce artificial diffusion in streamline direction only, (2) interpret this as a modification of the test function of the advection terms, (3) enforce consistency so that this modified test function is applied to all terms of the weak form. The SUPG method has been applied to various other problems, e.g., coupled multidimensional advective–diffusive systems [25], first-order linear hyperbolic systems [26] or first-order hyperbolic systems of conservation laws [27]. Because of its structural simplicity, generality and the quality of numerical solutions, the SUPG method has attracted considerable attention over the past two decades and many theoretical and computational results have been published. The major part of the theoretical analysis of the SUPG has been done by Johnson [26]. Motivated from mathematical analysis, another type of stabilization scheme, the Galerkin/Least-Squares (GLS) method, has been established. The GLS method is similar to the SUPG method in certain aspects. For linear interpolation functions, the two become identical. In the GLS method, least-squares forms of the residuals are added to the Galerkin method, enhancing stability of the Galerkin method without giving up consistency or degrading accuracy [28].

Another approach, the Residual-Free Bubbles (RFB) method [29–32], which is based on enriching the finite element space, has been recently introduced to solve the advection-dominated elliptic problems. The bubble functions are defined to be as rich as possible within an element. In other words, these functions are assumed to satisfy strongly the PDE in the interior of the element, up to the contribution of the piecewise polynomial functions. In practice, unless in very special situations (one-dimensional problems, limit cases, etc.), they require the actual solution of PDE problems (the bubble problems) in each element. An intuitive description of the RFB method is to find a cheap way to compute approximately the solution of the bubble problem in each element. This provides, as a consequence, an effective way to calculate good approximations for the optimal values of the stabilization parameters. The Pseudo Residual-Free Bubble (PRFB) method aims to get sub-grid nodes to approximate bubble functions cheaply using piecewise linear functions. The PRFB method also fits into the general stabilization method framework as the SUPG method, but differs in the stabilizing parameters and the operators on unknown variables and testing functions. For the stabilizing parameters of the PRFB method we refer to recent studies [32–36] which are restricted in one-dimensional and two-dimensional cases. Since our numerical experiments are based on a 3D ion channel, we have done derivations on the stabilizing parameters under specific choices of subgrid.

The SUPG, GLS and PRFB stabilizations are most frequently applied to fluid problems, such as Stokes and incompressible Navier–Stokes equations [37–40,32]. The SUPG scheme was used to simulate ion flow through a nanopore [41], in which, a "Fast SUPG" scheme was presented for SMPNP equations because the standard SUPG is expensive to evaluate for the SMPNP equations. In this work, we will try to study and implement two stabilized finite element algorithms for solving the 3D PNP/SMPNP equations for models based on experimentally determined ion channel structures, which, to our knowledge, have not been applied in computational biology.

In this paper, we describe a robust parallel FEM solver for both PNP and SMPNP equations for the simulation of ion transport through large ion channel systems, which can handle irregular geometries and complex boundary conditions. We found that the SUPG and PRFB schemes have good performance for solving PNP and SMPNP equations, even if there exists strong electrostatic potential around the molecule.

This paper is organized as follows. The PNP model and the stabilized FE schemes are introduced in the section Numerical Methods. First, we briefly review the 3D ion channel model and the PNP equations. Then, we present the robust stabilized finite element algorithms for solving the coupled nonlinear discretized equations. In the section Numerical experiments, we present some numerical results and assess the performance of our ion channel simulator in ion transport simulations. The solver is applied to VDAC and PA ion channel, and the simulation results are compared with our previous results [12]. The paper ends with the section Summary.

2. Numerical methods

2.1. The PNP and SMPNP equations

The PNP model combines the Nernst–Planck theory describing electrodiffusion of ions in the transmembrane channel with the Poisson theory describing the electrostatic potential whose gradient serves as a driving force of the ion motion. Consider an open domain $\Omega \in \mathbb{R}^3$, $\overline{\Omega} = \overline{\Omega}_m \cup \overline{\Omega}_s$, where Ω_m represents the protein and membrane region and Ω_s represents the solvent reservoirs and the channel region. The PNP equations couple the Nernst–Planck equations

$$\frac{\partial c_i}{\partial t} = \nabla \cdot D_i(\nabla c_i + \beta q_i c_i \nabla \phi), \quad x \in \Omega_s,\ 1 \le i \le N, \tag{1}$$

and the electrostatic Poisson equation:

$$-\nabla \cdot (\epsilon \nabla \phi) = \lambda \sum_i q_i c_i + \rho^f, \quad x \in \Omega, \tag{2}$$

where $c_i(x, t)$ is the concentration of the ith ion species carrying charge q_i. D_i is the spatial-dependent diffusion coefficient, and ϕ is the electrostatic potential. N is the number of diffusive ion species in the solution that are considered in the system. The constant $\beta =$

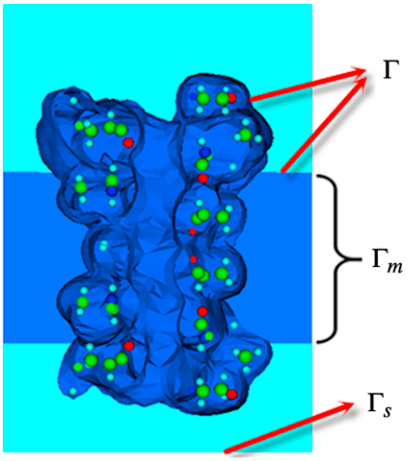

Fig. 1. A 2D cut through the center of the simulation box along the z axis illustrates the mesh representation of the protein and the membrane. This figure is obtained by using VCMM [46].

$1/(k_BT)$ is the inverse Boltzmann energy where k_B is the Boltzmann constant and T is the absolute temperature. We assume that the dielectric permittivity is piecewisely constant with $\epsilon = \epsilon_m\epsilon_0$ in Ω_m and $\epsilon = \epsilon_s\epsilon_0$ in Ω_s, where ϵ_0 is the dielectric constant of vacuum. In continuum treatments, typical values of ϵ_m and ϵ_s are 2 and 80, respectively. However, serious errors due to this assumption $\epsilon_m = 2$ have been known for some time. More studies on dielectric coefficients have been done [42–44]. The permanent (fixed) charge distribution

$$\rho^f(x) = \sum_j q_j\delta(x - x_j)$$

is an ensemble of singular atomic charges q_j located at x_j inside biomolecules. The characteristic function λ is equal to 1 in Ω_s and 0 in Ω_m, implying that mobile ions are present only in the solvent region.

The SMPNP equations add a nonlinear term to each of the Nernst–Planck equations to model the steric repulsion [45]:

$$\frac{\partial c_i}{\partial t} = \nabla\cdot D_i\left(\nabla c_i + \beta q_i c_i\nabla\phi + \frac{k_i c_i}{1-\sum_l a_l^3 c_l}\sum_l a_l^3\nabla c_l\right),$$

$$x\in\Omega_s,\ 1\le i\le N, \tag{3}$$

$$-\nabla\cdot(\epsilon\nabla\phi) = \lambda\sum_i q_i c_i + \rho^f,\quad x\in\Omega \tag{4}$$

where $k_i = \frac{a_i^3}{a_0^3}$ and a_i denotes the size of the ith ion species and a_0 of the water molecule.

2.2. The model system

A primary focus of this paper is the application of stabilized PNP solver to ion channel systems, wherein we compute the ionic current through a pore in a channel membrane. The model system is shown in Fig. 1, which consists of a protein, a membrane surrounding it, and a simulation box. Here the membrane is represented as a slab and no charge is assigned to the membrane in the present work. We use Γ to denote the interface between the two regions, such that $\overline{\Gamma} = \overline{\Omega}_m\cap\overline{\Omega}_s$, and Γ_m to denote the membrane boundary on the simulation box.

The electrical current across the pore can be calculated as:

$$I = -\sum_i q_i\int_S D_i\left(\frac{\partial c_i}{\partial z} + \frac{q_i}{k_BT}c_i\frac{\partial\phi}{\partial z}\right)dxdy, \tag{5}$$

where S is a cut plane at any cross section inside the pore. The ionic conductance can be obtained as follows:

$$G = \frac{I}{V}. \tag{6}$$

The PNP equations are solved with the following boundary conditions. Fixed electric potentials and ion concentrations are set on the upper and lower faces of the computational box. The channel is normal to these two faces (along the z-axis). On the lateral faces the potential is a linear function of the vertical coordinate. The concentrations of the positively and negatively charged ions are equal to each other on both top and bottom faces to ensure charge neutrality in the reservoirs. Additionally, there is a flux-free boundary surrounding the protein and membrane that prevents ions from penetrating through the region occupied by the protein and lipids, i.e.,

$$D_i(\nabla c_i + \beta q_i c_i\nabla\phi)\cdot n = 0,\quad \text{on } \Gamma$$

where n is the unit normal on the surface Γ.

2.3. Regularization of PNP equations

In this paper, only the steady state PNP equations are considered. An effective strategy for solving equation (2) is to decompose the solution of the Poisson equation into a singular component, a harmonic component and a regular component [17], i.e., $\phi = \phi^s + \phi^h + \phi^r$. The singular component ϕ_s is the restriction on Ω_m of the solution of

$$-\epsilon_m\Delta\phi^s(x) = \rho^f(x),\quad x\in\mathbb{R}^3, \tag{7}$$

and the harmonic component ϕ^h is the solution of a Laplace equation:

$$-\Delta\phi^h(x) = 0,\quad x\in\Omega_m, \tag{8}$$
$$\phi^h(x) = -\phi^s(x),\quad x\in\Gamma\cup\Gamma_m.$$

It is seen that $\phi^s(x)$ can be given analytically by the sum of Coulomb potentials. This $\phi^s(x)$ is then used to compute the boundary condition for $\phi^h(x)$, the latter is to be solved numerically from Eq. (8), for which we use finite element methods in this study. Subtracting these two components from Eq. (2), we get the governing equation for the regular component $\phi^r(x)$:

$$-\nabla\cdot(\epsilon\nabla\phi^r(x,t)) = \lambda\sum_i q_i c_i(x,t),\quad x\in\Omega, \tag{9}$$

and the interface conditions

$$\phi_s^r - \phi_m^r = 0,$$
$$\epsilon_s\frac{\partial\phi_s^r}{\partial n} - \epsilon_m\frac{\partial\phi_m^r}{\partial n} = \epsilon_m\frac{\partial(\phi^s+\phi^h)}{\partial n},\quad x\in\Gamma.$$

It is worth noting that there is no decomposition of the potential in the solvent region, thus $\phi(x) = \phi^r(x)$ in Ω_s. For the steady-state of the system, the final regularized Poisson–Nernst–Planck equations consist of the regularized Poisson equation (9) and the steady-state Nernst–Planck equations

$$\nabla\cdot D_i(x)(\nabla c_i(x) + \beta q_i c_i(x)\nabla\phi^r(x)) = 0,\quad x\in\Omega_s. \tag{10}$$

2.4. Stabilized FE methods for the NP equations

In this section, we will briefly present the standard SUPG and Pseudo Residual-free Bubbles stabilization methods to solve NP equations. Additionally, we use a standard finite element discretization for solving the Poisson equation, of which more details and discussion can be found in Ref. [12].

2.4.1. The SUPG method

In the presence of a strong electrostatic potential, the Nernst–Planck equations have a large drift term, which is a challenge to standard Galerkin methods. One remedy is to augment the Galerkin weak form by adding artificial dissipative terms to stabilize the method. The SUPG scheme introduces a certain amount of artificial diffusion in streamline direction only to avoid the oscillations in advection-dominated problems. In this section, we briefly present the SUPG stabilization method to solve the NP equations. Let us recall the standard Galerkin method. The weak form of (10) is approximated as follows:

Let $u = \phi^r$, for each i, $1 \le i \le N$, find $c_i \in H_a^1(\Omega_s)$ which satisfies

$$\int_{\Omega_s} D_i(\nabla c_i \nabla v + \beta q_i c_i \nabla u \nabla v) d\Omega_s = 0, \quad \forall v \in H_c^1(\Omega_s), \tag{11}$$

where $H_a^1(\Omega) = \{c_i \in H^1(\Omega) \mid c_i = \eta_i \text{ on } \Gamma_s\}$, here η_i denotes the Dirichlet boundary function, and $H_c^1(\Omega) = \{c_i \in H^1(\Omega) \mid c_i = 0 \text{ on } \Gamma_s\}$.

To simplify the presentation of the SUPG scheme, we denote the standard weak form by

$$B(c_i, v) = \int_{\Omega_s} D_i(\nabla c_i \nabla v + \beta q_i c_i \nabla u \nabla v) dx, \tag{12}$$

and the stabilization form by

$$S(c_i, v_{\text{supg}}) = \sum_K \int_K \left(\nabla \cdot D_i(\nabla c_i + \beta q_i c_i \nabla u)\right) \cdot v_{\text{supg}} dx. \tag{13}$$

Then the weak form of the Nernst–Planck equation using the SUPG scheme is as follows:

For each i, $1 \le i \le N$, find $c_i \in H_a^1(\Omega_s)$ which satisfies

$$B(c_i, v) + S(c_i, v_{\text{supg}}) = 0, \quad \forall v \in H_c^1(\Omega_s), \tag{14}$$

where the test functions v_{supg} in stabilized form are

$$v_{\text{supg}} = \sigma_K \mathbf{a_i} \cdot \nabla v. \tag{15}$$

We also isolate the Péclet number Pe with a stability parameter of the form [47]

$$\sigma_K = \frac{h_K}{2\|\mathbf{a_i}\|_2} \xi(\text{Pe}_K), \tag{16}$$

$$\mathbf{a_i} = -D_i \beta q_i \nabla u \tag{17}$$

where h_K denotes the diameter of the element K, and

$$\text{Pe}_K = \frac{\|\mathbf{a_i}\|_2 h_K}{6 D_i}, \tag{18}$$

$$\xi(\text{Pe}_K) = \begin{cases} \text{Pe}_K, & 0 \le \text{Pe}_K \le 1, \\ 1, & \text{Pe}_K \ge 1, \end{cases} \tag{19}$$

where Pe_K denotes the Péclet number of element K, which is an indication of the strength of advection. Specifically, a Péclet number greater than 1 indicates that advection is dominating the flow and that stabilization may be necessary.

The convergence rate of the L_2 error for the SUPG scheme is typically half an order less than the Galerkin method [48]. That is, the convergence rate of the L_2 error is $O(h^{k+1/2})$ for the SUPG scheme, and $O(k^{k+1})$ for the Galerkin method, where k refers to the polynomial degree of the approximating space. However, the benefit of the SUPG method lies in its stability properties. The SUPG scheme leads to a more reasonable numerical solution, compared to the Galerkin method, even for coarse meshes.

A possible drawback of the SUPG method is the sensitivity of the solution to the stabilization parameter σ_K, whose value is not determined precisely by the available theory. A way to recover intrinsically the value of σ_K is to use the residual-free bubbles (RFB) approach [35] which will be applied to solve PNP equations in the next section.

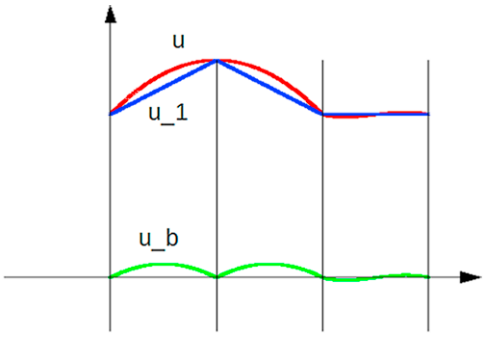

Fig. 2. One dimension residual-free bubbles.

2.4.2. The pseudo residual-free bubbles method

Both of SUPG and residual-free bubbles (RFB) are closely related methods that have been used to stabilize the simulation. The idea of RFB is to enlarge the finite element space V_L in the following way. For each simplex K, we define the space of bubbles in K as $B^K = H_0^1(K)$, the enlarged space $V_B = \bigoplus B^K$, and sets

$$V_h = V_h^{\text{RFB}} = V_L \bigoplus V_B. \tag{20}$$

Then the weak form of the ith Nernst–Planck equations using residual-free bubbles (RFB) is approximated as follows:

Find $c_h^i = c_L^i + c_b^i \in V_L \bigoplus V_B$ such that: for all $v_L \in V_L$, $K \in \mathcal{T}_h$, and $v_b^k \in B^K$,

$$a(c_L^i + c_b^i, v_L) = 0, \qquad a_K(c_L^i + c_b^{K,i}, v_b^K) = 0, \tag{21}$$

where $a(c_i, v) = \int_{\Omega_s} D_i(\nabla c_i \nabla v + \beta q_i c_i \nabla u \nabla v) d\Omega_s$ and the subscript in $a_K(\cdot,\cdot)$ and $(\cdot)_K$ indicates the integrals involved are restricted to the simplex K. Since V_h is infinite-dimensional, approximate methods are introduced by [35,34,36]. The second equation of

Eq. (21) implies the PDE is local, i.e.:

$$\nabla \cdot D_i(\nabla c_b^{K,i} + \beta q_i c_b^{K,i} \nabla u) = -\nabla \cdot D_i(\nabla c_L^i + \beta q_i c_L^i \nabla u) \quad \text{in } K, \tag{22}$$

$$c_b^{K,i} = 0 \quad \text{on } \partial K. \tag{23}$$

Residual-free bubbles $c_b^{K,i}$ are the functions satisfying these equations strongly. In one-dimensional problems, with continuous solution of unknown variable u (without loss of generality and here the u is not related to the PNP equations), the approximation is exact (see Fig. 2), i.e. $u = u_h = u_1 + u_b$.

Note that in our numerical cases, u is piecewise linear so that ∇u is piecewise constant, therefore the solution of this PDE is spanned by a single bubble basis function if we suppose D_i is a piecewise constant:

$$c_b^{K,i} = c_K \varphi_K. \tag{24}$$

Without any loss of generality, φ_K solves:

$$\nabla \cdot D_i(\nabla \varphi_K + \beta q_i \varphi_K \nabla u) = 1 \quad \text{in } K, \tag{25}$$

$$\varphi_K = 0 \quad \text{on } \partial K. \tag{26}$$

Essentially, all stabilization methods add a stabilizing term to the original Galerkin formulation of the problem [49]. Eq. (27) shows the stabilizing term can be written as L^2 products within each element, which involve the residual of the equation and an

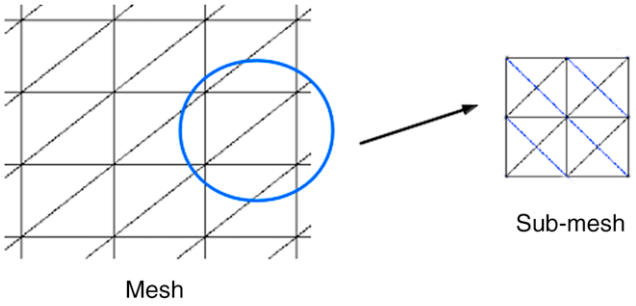

Fig. 3. Two-dimensional two-level mesh.

operator applied to the test function, the former being multiplied by a numerical parameter.

$$a(c_L^i, v_L) + \sum_K \hat{\tau}_K \int_K \mathcal{R}(c_L^i)\mathcal{P}(v_L) = 0. \tag{27}$$

In this paper, $\mathcal{R}(c_h^i) = \nabla \cdot D_i(\nabla c_h^i + \beta q_i c_h^i \nabla u)$, $\mathcal{P}(v_h) = \nabla \cdot D_i(\beta q_i v_h \nabla u)$. If we define an operator M_K in each simplex K as for any given right-hand side g, say, there is a unique solution $\varphi := M_K(g)$ satisfying

$$\nabla \cdot D_i(\nabla\varphi + \beta q_i \varphi \nabla u) = g \quad \text{in } K, \qquad \varphi = 0 \quad \text{on } \partial K. \tag{28}$$

Then the $\hat{\tau}_K$ in Eq. (27) can be written as

$$\hat{\tau}_K = \frac{1}{|K|}\int_K M_K(1), \tag{29}$$

where $|K|$ is the volume of the simplex. To get the numerical value of $\hat{\tau}_K$, the basic idea is to construct a submesh in each element K and solve the problem on the augmented space, essentially made of piecewise linear functions on the augmented mesh. More precisely, two-level meshes can be constructed as in Fig. 3 to solve Eqs. (25) and (26). Then the linear approximations in the submeshes can be used to replace $M_K(1)$ in the integrals.

We are going to take a submesh that contains just one additional node P_K in each element K. The node P_K is then joined to the four vertices and the tetrahedron is split into four tetrahedra (see Fig. 4 (left)).

Papers about the PRFB method provide strategies to find sub-optimal P^* by discussing various inflow edges/faces numbers [35,36]. Note that they prescribe very strong conditions such as P^* should be along the median from V_i in two-dimensional cases [35,36]. Since the exact optimized P^* is nontrivial to be obtained, we assign P^* as the gravity center in each element K and compute $\hat{\tau}_K$ by cheap calculations.

As described above, the additional node P^* splits the tetrahedron into four sub-tetrahedra. For each sub-tetrahedron, numerical value in the face opposite to the node P_K is set as 0, Fig. 4 (right) illustrates the numerical value distribution in the sub-simplex via linear interpolations (the value on P^* is set as 1) without loss of generality.

If we define the numerical solution on P^*, $\varphi_K(P^*)$, as an approximation of $M_K(1)|_{P^*}$, then we have

$$\begin{aligned}\hat{\tau}_K &= \frac{1}{|K|}\int_K M_K(1) = \frac{1}{|K|}\sum_{i=1}^4 \int_{K_i} M_K(1)\\ &= \frac{1}{|K|}\sum_{i=1}^4 \int_0^1 \frac{1}{3}(t^2 S_i)(tH_i)\varphi_K(P^*)dt\\ &= \frac{1}{|K|}\sum_{i=1}^4 \frac{1}{4}|K_i|\varphi_K(P^*)\\ &= \frac{1}{4}\varphi_K(P^*)\end{aligned} \tag{30}$$

where S_i denotes the area of the ith face of element K and H_i denotes its height.

To obtain the finite element approximations on P^* in each element K, we build a 5×5 stiffness matrix using linear elements as following:

$$\begin{pmatrix} A_{11} & A_{12} & A_{13} & A_{14} & A_{15}\\ A_{21} & A_{22} & A_{23} & A_{24} & A_{25}\\ A_{31} & A_{32} & A_{33} & A_{34} & A_{35}\\ A_{41} & A_{42} & A_{43} & A_{44} & A_{45}\\ A_{51} & A_{52} & A_{53} & A_{54} & A_{55}\end{pmatrix}\begin{pmatrix}\varphi_K(V_1)\\ \varphi_K(V_2)\\ \varphi_K(V_3)\\ \varphi_K(V_4)\\ \varphi_K(P^*)\end{pmatrix} = \begin{pmatrix} b_1\\ b_2\\ b_3\\ b_4\\ b_5\end{pmatrix}. \tag{31}$$

Note that the Dirichlet condition is set on ∂K, i.e., $\varphi_K(V_i) = 0$, $i = 1, \ldots, 4$. Define $\Phi^i_{P^*}$ as one of the basis functions in K_i such that $\Phi^i_{P^*}(V_j) = 0$, $j = 1, \ldots, 4 (j \neq i)$ and $\Phi^i_{P^*}(P*) = 1$, then the linear problem comes to

$$A_{55}\varphi_K(P^*) = b_5, \tag{32}$$

where

$$A_{55} = \sum_{i=1}^4 \int_{K_i} \hat{D}(P^*)(\nabla\Phi^i_{P^*}\nabla\Phi^i_{P^*} + \beta q_i \Phi^i_{P^*}\nabla u \nabla \Phi^i_{P^*})dK_i \tag{33}$$

and

$$b_5 = \sum_{i=1}^4 \int_{K_i} \Phi^i_{P^*} dK_i = \frac{1}{4}|K|. \tag{34}$$

The solution of $\hat{\tau}_K$ can be obtained via substituting Eqs. (33) and (34) to Eq. (32) and it comes to

$$\begin{aligned}\hat{\tau}_K &= \frac{1}{4}\varphi_K(P^*) = \frac{b_5}{4A_{55}}\\ &= \frac{|K|}{16\sum_{i=1}^4 \int_{K_i}\hat{D}(P^*)(\nabla\Phi^i_{P^*}\nabla\Phi^i_{P^*} + \beta q_i\Phi^i_{P^*}\nabla u\nabla\Phi^i_{P^*})dK_i}.\end{aligned} \tag{35}$$

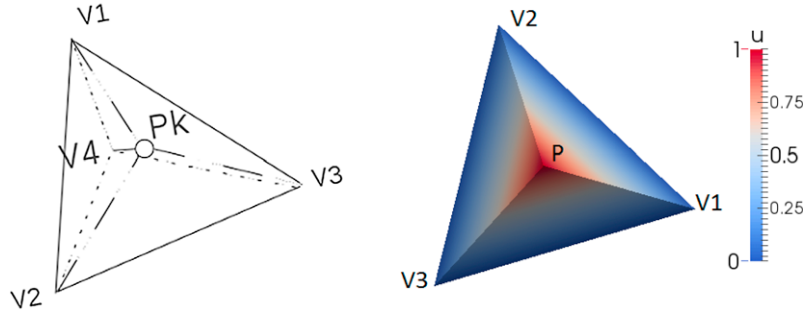

Fig. 4. Subgrid contains just one addition node in the gravity center. (left) Additional node P_K splits the tetrahedron into four tetrahedra. (right) Linear interpolations in sub-tetrahedra.

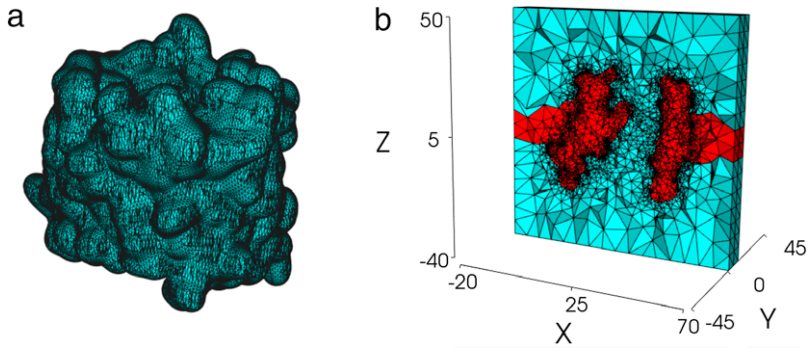

Fig. 5. (a) Triangular boundary mesh conforming to the VDAC ion channel surface. (b) A view of cross section of the whole tetrahedral volume mesh.

Since ∇u is piecewise constant in each element K, Eq. (33) can be computed analytically using the coordinates of the four vertices. But in practice, we simply compute it using numerical quadrature, which can be more easily extended to higher order schemes.

Since the gradient of the basis functions is piecewise constant in each element K, we can estimate $\hat{\tau}_k$ in the following way:

$$\begin{aligned}\hat{\tau}_K &= \frac{|K|}{16\sum_{i=1}^{4}\int_{K_i}\hat{D}(P^*)(\nabla\Phi^i_{P^*}\nabla\Phi^i_{P^*}+\beta q_i\Phi^i_{P^*}\nabla u\nabla\Phi^i_{P^*})dK_i}\\ &\approx \frac{|K|}{16\sum_{i=1}^{4}\int_{K_i}\hat{D}(P^*)\left(\frac{C_1}{h_K^2}+\frac{C_2\Phi^i_{P^*}}{h_K^2}\right)dK_i}\\ &\approx \frac{|K|}{4\hat{D}(P^*)\left(\frac{C_3}{h_K^2}\right)|K|}\\ &\approx O(h_K^2),\end{aligned} \tag{36}$$

where h_K denotes the diameter of the element K. It is found that the definition of $\hat{\tau}_K$ from the PRFB approach has the same order of h_K as from the SUPG approach, but different in the formulation.

Assigning P as the center of gravity is reasonable, which relies on the following reasons: (i) It is consistent with two-level mesh method just adding one additional point P_K in each element K; (ii) Adding the gravity center into the tetrahedron ensures certain quality of the submesh; (iii) The strategies to find the optimized P^* have strong assumptions to reduce the complexity, for example, they assume P^* is along the median of a triangle, and by doing so, a sub-optimal solution is easily obtained.

Those two stabilization methods can be implemented for SMPNP equations in a similar manner. We found that the additional terms in SMPNP only make a small contribution to the total flux in a channel system, therefore the main numerical difficulties for both PNP and SMPNP are due to the same dominating drift term, and our tests also showed that SUPG and PRFB have similar performance for SMPNP equations (data not shown here). Because SMPNP is not the focus of the paper, we omit more details about the application of stabilization methods to SMPNP equations here.

3. Numerical experiments

In this section we apply our stabilized FEM to solve PNP equations for simulations of ion transport through two proteins, VDAC and PA ion channels. In our previous work, the standard FEM solver works well for the simulation of VDAC ion channel [12]. However, it fails for the biggest ion channel (PA ion channel) listed in article [23]. To verify the effectiveness of our new solver, we apply it to VDAC and PA ion channels to compare the electrostatic potential, ion concentrations and conductances under various combinations of inputs. The computations were carried out on the cluster LSSC-III of the State Key Laboratory of Scientific and Engineering Computing of China, which consists of compute nodes with dual Intel Xeon X5550 quad-core CPUs, interconnected via DDR InfiniBand network. To solve PNP equations, the stabilized FEM costs almost the same time as the standard FEM. More details about the efficiency of the standard FEM were discussed in our previous work [12]. Actually, for the simulation of the PA ion channel, the whole computation time is about 2 h. For VDAC ion channel, it costs much less than 2 h.

3.1. Numerical test with VDAC ion channel

The voltage-dependent anion channels are 30-kDa transmembrane (TM) proteins found in the outer membrane of mitochondria. The VDAC serves an essential role in the transport of metabolites and electrolytes between the cell matrix and mitochondria. Among three isoforms found in many eukaryotic cells, the prototype isoform, VDAC1, shares a sequence identity up to 75% and the characteristic electrophysiological features. The atomic-resolution structure of VDAC1 ion channel is obtained from the protein data bank (code 2JK4) [50]. The partial charges and atomic radii for each atom in the protein are obtained by converting the PDB file to the PQR format using PDB2PQR software [51]. The PQR file of VDAC1 contains 4393 atoms, which is used to generate the surface mesh using our program TMSmesh [52,53]. Then the tetrahedral volume mesh is generated using our meshing tool chain [12]. Finally, the membrane region is extracted and the involved tetrahedra and boundary faces are properly marked, which ends the mesh construction for the whole ion channel systems. Fig. 5 shows an example of the unstructured tetrahedral volume mesh and triangular surface mesh of the VDAC ion channel.

The membrane and protein regions are described by a low relative dielectric constant $\epsilon_m = 2$. A high relative dielectric constant $\epsilon_s = 80$ is assigned to the aqueous region, i.e., the volume outside of the protein-membrane region. The diffusion coefficients for cation and anion, e.g., K^+ and Cl^-, in the bulk region are set to their experimental values: $D_{Cl} = 0.203$ Å^2/ps, $D_K = 0.196$ Å^2/ps. However, there are no experimental data available for the diffusion coefficient in the channel pore. The diffusion coefficients are likely to vary substantially near the protein surface in the pore. Some studies about this issue have been reported [54,55,23]. Here we use a smooth transient function to represent the diffusion coefficient near the channel entrance [12,56], and we obtain the diffusion coefficient in channel pore through matching the experimental data, i.e., the current value at $V = 100$ mV. We set $0.4D_K$ and $0.4D_{Cl}$ as the diffusion coefficients in pore region which are used for the simulation.

The voltage applied to the system, V_{applied}, is given by the potential difference between the top and bottom boundaries. Ion

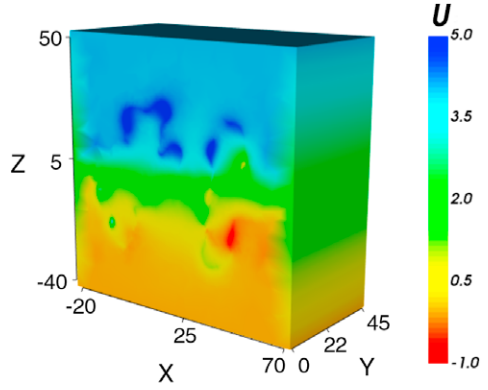

Fig. 6. A cross sectional view of the electrostatic potential obtained from PNP calculation with $V_{\text{applied}} = 100$ mV and $c_{i,\text{bulk}} = 1.0$ M.

Table 1
The current obtained from the simulation of VDAC1 channel by using SUPG scheme, PRFB method and Galerkin method.

Voltage (mV)	Current (pA)		
	SUPG	PRFB	Galerkin
−50	−27.2	−27.6	−27.6
−40	−10.3	−10.7	−10.6
−30	6.2	6.0	5.9
−20	22.3	22.2	22.2
−10	38.0	38.1	38.1
0	53.1	53.3	53.4
10	67.8	68.4	68.4

concentrations on the top and bottom side boundaries are set to their bulk values $c_{i,\text{bulk}}$.

For a given boundary condition ($V_{\text{applied}} = 100$ mV and $c_{i,\text{bulk}} = 1.0$ M), the PNP equations are solved by using the SUPG scheme and the PRFB method to obtain the steady-state ion concentrations and electrostatic potential. A cross sectional view of the potential of the whole domain region is shown in Fig. 6.

To obtain the current across the pore and compare with our previous results [12], the PNP equations are computed for a variety of voltages by using the SUPG scheme and the PRFB method. Table 1 shows the current obtained from the SUPG scheme, the PRFB method and the standard Galerkin method for the simulation of VDAC1 in the asymmetric 0.1:1.0 M KCl solution. It is seen that the simulation results of the PRFB method are closer to results of the Galerkin method than that of the SUPG scheme. Table 3 summarizes the conduction properties of VDAC1 obtained from PNP simulation, BD simulation [23] and experimental data. It is seen that the PNP simulation results agree well with BD simulation results and experimental results.

Except for analysis of the electrostatic potential, current and ion conduction properties using different numerical approaches, we also observe the iterations between the NP and the PE and the corresponding CPU time during the whole calculations to compare the efficiency of these methods. Table 2 lists the iteration number and CPU time of SUPG and PRFB respectively by setting stopping criterion $tol = 10^{-8}$. Overall, both methods solve the VDAC1 case efficiently via several tens iterations and the whole calculations can be completed in $2 \approx 3$ min. Nonetheless, from Table 2, it is found that the PRFB method costs a little more iterations than the SUPG approach, but is more stable than the SUPG method in different numerical tests with changing voltage values.

3.2. Numerical test with PA ion channel

The PA is a key component of the anthrax toxin, as it allows entry of the enzymatic components edema factor and lethal factor into the host cell, through the formation of a membrane spanning pore. After proteolytic activation on the host cell surface, PA forms a membrane-inserting heptamer that translocates the toxic enzymes, edema factor and lethal factor, into the cytosol [57,58]. Each monomer of the channel contains 7 His residues and the net charge of the channel can be either $7e$ with all unprotonated His (denoted by HSD) or $21e$ with all protonated His (HSP). Low pH condition used to enhance the pore formation in the experiment may protonate His near the trans-side bath, but the exact protonation state of each His is yet to be determined. Currently, only a computational model structure (PDB:1V36) [59] has been reported. The partial charges and atomic radii for each atom in the protein are obtained by using the PDB2PQR software. Here we choose the structure with all unprotonated His ($7e$) for the following simulations. The PQR file of PA channel contains 62 277 atoms. The surface and volume meshes of PA channel are shown in Fig. 7. The mesh over the whole domain has a total of 257 899 vertices and 1 628 920 tetrahedra.

Table 2
The iterations and CPU time cost from the simulation of VDAC1 channel by using SUPG scheme and PRFB method respectively.

Voltage (mV)	SUPG		PRFB	
	Iters	CPU time (s)	Iters	CPU time (s)
−50	69	143.6	79	158.4
−40	69	146.2	78	156.6
−30	71	147.4	77	153.0
−20	72	149.9	77	153.7
−10	74	150.6	78	153.4
0	75	153.8	78	152.5

Table 3
Ion conduction properties of VDAC1: Conductance (G), ion selectivity from current ratio ($G_{\text{Cl}}/G_{\text{K}}$).

Method	Voltage (mV)	G	$G_{\text{Cl}}/G_{\text{K}}$
PNP	−100	3.68	1.79
	+100	3.21	1.41
BD	−100	3.77 ± 0.11	1.92
	+100	3.15 ± 0.09	1.94
Exp.		3.9–4.5	

In our previous work, we found that the PNP solver with standard Galerkin method could not get convergent results for the simulation of PA ion channel. Here we use the SUPG scheme and the PRFB method to solve PNP equations for the simulation of ion transport through PA ion channel system. Similar as in the numerical test on VDAC channel, we use the following parameters: $\epsilon_m = 2$, $\epsilon_s = 80$, the diffusion coefficients for K^+ and Cl^-, $D_{\text{Cl}} = 0.203$ Å^2/ps, $D_{\text{K}} = 0.196$ Å^2/ps in bulk region, $0.4D_{\text{K}}$ and $0.4D_{\text{Cl}}$ in the channel pore region.

We compare the ion conduction properties of PA via stabilized FEMs, BD and experimental data in Table 4. Both PNP simulation results and BD simulation results show much higher conductance than the experimental data [60]. Because the calculated electrophysiological properties substantially deviate from available experimental data, the present study suggests that further structural refinement and determination of His protonation state are required for PA. Such structural refinement will facilitate the understanding of the channel conducting mechanism.

Fig. 8 elucidates the electrostatic potential at the center of the PA channel plotted along z-axis obtained from the PNP calculation by using SUPG and PRFB methods with $V_{\text{applied}} = 100$ mV, $c = 1.0$ M (solid) and $V_{\text{applied}} = 100$ mV, $c = 0.5$ M (dashed). It is seen that the potential obtained from SUPG and PRFB methods is almost the same but disparate slightly in the pore area. Moreover, we found that the potential with a higher concentration boundary condition is larger than that with a lower concentration boundary condition in the channel pore region due to ionic screening effect.

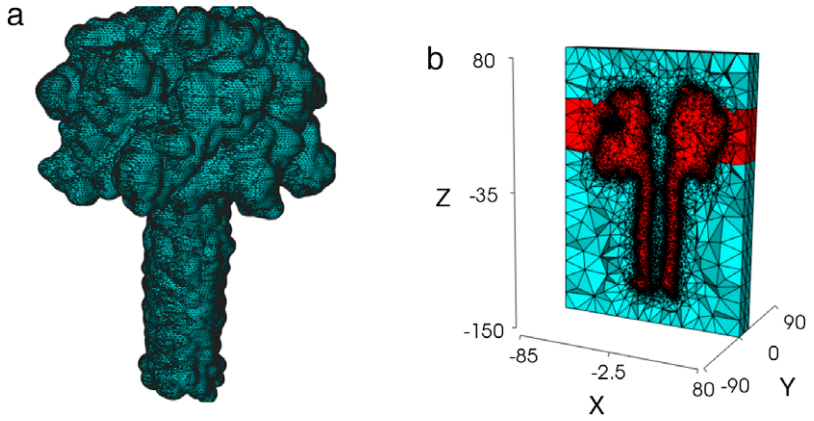

Fig. 7. (a) Triangular boundary mesh conforming to the PA ion channel surface. (b) A view of cross section of the whole tetrahedral volume mesh.

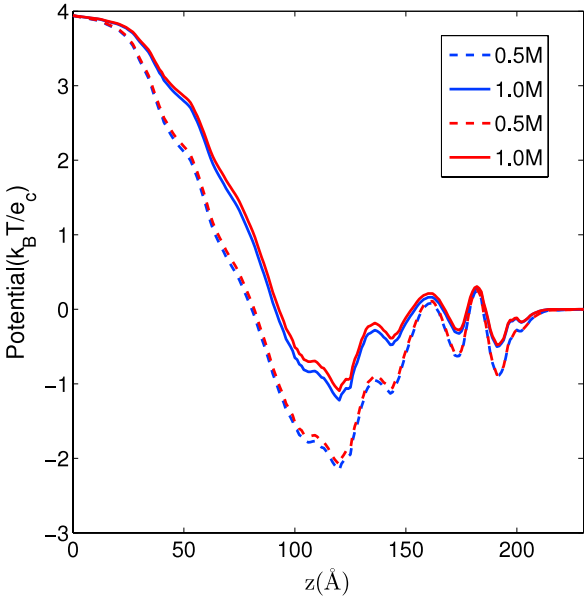

Fig. 8. Electrostatic potential at the center of the PA channel plotted along z-axis obtained from the PNP calculation by using SUPG scheme (blue) and PRFB method (red) with $V_{\text{applied}} = 100$ mV, $c = 1.0$ M (solid) and $V_{\text{applied}} = 100$ mV, $c = 0.5$ M (dashed). (For interpretation of the references to color in this figure legend, the reader is referred to the web version of this article.)

Table 4
Ion conduction properties of PA: Conductance (G), ion selectivity from current ratio ($G_{\text{Cl}}/G_{\text{K}}$).

Method	Voltage (mV)	G (nS)	$G_{\text{K}}/G_{\text{Cl}}$
PNP	−100	0.58	21.2
	+100	0.35	5.16
BD	−100	0.93 ± 0.04	22.3
	+100	1.48 ± 0.05	13.8
Exp.		0.17–0.20	

4. Summary

In this paper, we describe a stabilized FEM solver for both PNP and SMPNP simulations of ion transport through large ion channel systems. Two stabilized schemes, SUPG and PRFB are introduced to enhance numerical robustness. Numerical tests are carried out on the VDAC and PA channels. The simulation results obtained with the stabilized schemes agree well with the Galerkin method, especially for the results of the PRFB method in our numerical experiments. These two stabilizing methods succeeded in the simulation of PA channel which our previous solver failed to simulate. The simulations of PA channel suggest that further structural refinement of the channel is required for proper analysis of the system. In practice, the stabilized algorithms are necessary when solving large proteins. Within our test data set, PRFB is slightly more accurate and stable than SUPG, while SUPG is relatively more convenient to implement. However, the stabilized methods cannot overcome all the numerical challenges, and may fail in particular difficult cases, such as for huge molecular systems and when the mesh quality is very poor. These issues will be the subjects of future explorations. In addition, the PRFB method in this article selects the gravity center in each element to calculate the stabilizing coefficient $\hat{\tau}_k$, which can be improved via computing more optimized P^* in certain ways.

Acknowledgments

We would like to thank Shiyang Bai for his great help. B. Tu and B.Z. Lu are supported by the State Key Laboratory of Scientific/Engineering Computing, National Center for Mathematics and Interdisciplinary Sciences, the Chinese Academy of Sciences, the China NSF (91230106) and 863 program (2012AA020403). Y. Xie and L.B. Zhang are supported by National 973 Project of China (2011CB309703), National 863 Project of China (2012AA01A309), China NSF (11171334 and 11321061), and National Center for Mathematics and Interdisciplinary Sciences of Chinese Academy of Sciences.

References

[1] B. Hille, Ion Channels of Excitable Membranes, third ed., Sinauer, 2001.
[2] D. Marx, J. Hutter, Modern Methods and Algorithms of Quantum Chemistry, John von Neumann Institute for Computing, Jülich, 2000.
[3] S. Li, M. Hoyles, S. Kuyucak, S. Chung, Brownian dynamics study of ion transport in the vestibule of membrane channels, Biophys. J. 74 (1998) 37–47.
[4] B. Corry, S. Kuyucak, S.H. Chung, Tests of continuum theories as models of ion channels. II. Poisson–Nernst–Planck theory versus brownian dynamics, Biophys. J. 78 (2000) 2364–2381.
[5] S. Kuyucak, O.S. Andersen, S.H. Chung, Models of permeation in ion channels, Rep. Progr. Phys. 64 (2001) 1427–1472.
[6] D. Chen, J. Lear, R.S. Eisenberg, Permeation through an open channel: Poisson–Nernst–Planck theory of a synthetic ionic channel, Biophys. J. 72 (1997) 97–116.
[7] B.Z. Lu, Poisson–Nernst–Planck equations, Poisson–Nernst–Planck equations, in: B. Engquist (Ed.), Encyclopedia of Applied and Computational Mathematics, Springer-Verlag, Berlin, Heidelberg, 2014.
[8] O.J. Riveros, T.L. Croxton, W.M. Armstrong, Theoretical and computational models of biological ionchannels, J. Theoret. Biol. 140 (1989) 221–230.
[9] P.A. Markowich, The Stationary Semiconductor Device Equations, Springer-Verlag, Vienna, 1986.
[10] R.S. Eisenberg, Ionic channels in biological membranes: natural nanotubes, Acc. Chem. Res. 31 (1998) 117–123.

[11] B. Roux, T. Allen, S. Berneche, W. Im, Theoretical and computational models of biological ionchannels, Q. Rev. Biophys. 7 (1) (2004) 1–103.
[12] B. Tu, M. Chen, Y. Xie, L. Zhang, B. Eisenberg, B.Z. Lu, A parallel finite element simulator for ion transport through three-dimensional ion channel systems, J. Comput. Chem. 34 (2013) 2065–2078.
[13] M.G. Kurnikova, R.D. Coalson, P. Graf, A. Nitzan, A lattice relaxation algorithm for three-dimensional Poisson–Nernst–Planck theory with application to ion transport through the gramicidin a channel, Biophys. J. 76 (1999) 642–656.
[14] Q. Zheng, D. Chen, G.W. Wei, Second-order Poisson–Nernst–Planck solver for ion transport, J. Comput. Phys. 230 (13) (2011) 5239–5262.
[15] W. Kucza, M. Danielewski, A. Lewenstam, Eis simulations for ion-selective site-based membranes by a numerical solution of the coupled Nernst–Planck–Poisson equations, Electrochem. Commun. 8 (3) (2006) 416–420.
[16] T. Sokalski, A. Lewenstam, Application of Nernst–Planck and Poisson equations for interpretation of liquid-junction and membrane potentials in real-time and space domains, Electrochem. Commun. 3 (3) (2001) 107–112.
[17] B.Z. Lu, M.J. Holst, J.A. McCammon, Y.C. Zhou, Poisson–Nernst–Planck equations for simulating biomolecular diffusion–reaction processes I: finite element solutions, J. Comput. Phys. 229 (19) (2010) 6979–6994.
[18] B.Z. Lu, J.A. McCammon, Molecular surface-free continuum model for electrodiffusion processes, Chem. Phys. Lett. 451 (2008) 282–286.
[19] B.Z. Lu, Y.C. Zhou, G.A. Huber, S.D. Bond, M.J. Holst, J.A. McCammon, Electrodiffusion: a continuum modeling framework for biomolecular systems with realistic spatiotemporal resolution, J. Chem. Phys. 127 (13) (2007) 135102.
[20] Y. Xie, J. Cheng, B.Z. Lu, L. Zhang, Parallel adaptive finite element algorithms for solving the coupled electro-diffusion equations, Mol. Based Math. Biol. 1 (2013) 90–108.
[21] U. Hollerbach, D.P. Chen, R.S. Eisenberg, Two- and three-dimensional Poisson–Nernst–Planck simulations of current flow through gramicidin A, J. Sci. Comput. 16 (4) (2002) 373–409.
[22] S.R. Mathur, J.Y. Murthy, A multigrid method for the Poisson–Nernst–Planck equations, SIAM J. Appl. Math. 52 (17–18) (2009) 4031–4039.
[23] K.I. Lee, S. Jo, H. Rui, B. Egwolf, B. Roux, R.W. Pastor, W. Im, Web interface for Brownian dynamics simulation of ion transport and its applications to beta-barrel pores, J. Comput. Chem. 33 (3) (2012) 331–339.
[24] A.N. Brooks, T.J.R. Hughes, Streamline upwind/Petrov–Galerkin formulations for convection dominated flows with particular emphasis on the incompressible Navier–Stokes equations, Comput. Methods Appl. Mech. Engrg. (1990) 199–259.
[25] T.J.R. Hughes, M. Mallet, A new finite element formulation for computational fluid dynamics: III. The generalized streamline operator for multidimensional advective–diffusive systems, Comput. Methods Appl. Mech. Engrg. 58 (3) (1986) 305–328.
[26] C. Johnson, U. Nävert, J. Pitkäranta, Finite element methods for linear hyperbolic problems, Comput. Methods Appl. Mech. Engrg. 45 (1) (1984) 285–312.
[27] T.J. Hughes, T. Tezduyar, Finite element methods for first-order hyperbolic systems with particular emphasis on the compressible Euler equations, Comput. Methods Appl. Mech. Engrg. 45 (1) (1984) 217–284.
[28] T.J.R. Hughes, L.P. Franca, G.M. Hulbert, A new finite element formulation for computational fluid dynamics: VIII. The Galerkin/least-squares method for advective–diffusive equations, Comput. Methods Appl. Mech. Engrg. 73 (2) (1989) 173–189.
[29] J. Matsumoto, A relationship between stabilized fem and bubble function element stabilization method with orthogonal basis for incompressible flows, J. Appl. Mech. 8 (2005) 233–242.
[30] H.M. Mourad, J. Dolbow, I. Harari, A bubble-stabilized finite element method for Dirichlet constraints on embedded interfaces, Internat. J. Numer. Methods Engrg. 69 (4) (2007) 772–793.
[31] A. Coutinho, L. Franca, F. Valentin, Numerical multiscale methods, Internat. J. Numer. Methods Fluids 70 (4) (2012) 403–419.
[32] D. Nechaev, J. Schröter, M. Yaremchuk, A diagnostic stabilized finite-element ocean circulation model, Ocean Model. 5 (1) (2003) 37–63.
[33] L.P. Franca, A. Russo, Approximation of the Stokes problem by residual-free macro bubbles, East-West J. Numer. Math. 4 (1996) 265–278.
[34] F. Brezzi, D. Marini, E. Süli, Residual-free bubbles for advection–diffusion problems: the general error analysis, Numer. Math. 85 (1) (2000) 31–47.
[35] F. Brezzi, D. Marini, A. Russo, Applications of the pseudo residual-free bubbles to the stabilization of convection–diffusion problems, Comput. Methods Appl. Mech. Engrg. 166 (1) (1998) 51–63.
[36] F. Brezzi, L. Marini, A. Russo, On the choice of a stabilizing subgrid for convection–diffusion problems, Comput. Methods Appl. Mech. Eng. 194 (2) (2005) 127–148.
[37] M.A. Behr, L.P. Franca, T.E. Tezduyar, Stabilized finite element methods for the velocity–pressure-stress formulation of incompressible flows, Comput. Methods Appl. Mech. Engrg. 104 (1) (1993) 31–48.
[38] F. Brezzi, J. Douglas Jr., Stabilized mixed methods for the Stokes problem, Numer. Math. 53 (1–2) (1988) 225–235.
[39] G. Hauke, T. Hughes, A unified approach to compressible and incompressible flows, Comput. Methods Appl. Mech. Engrg. 113 (3) (1994) 389–395.
[40] G. Hauke, T.J. Hughes, A comparative study of different sets of variables for solving compressible and incompressible flows, Comput. Methods Appl. Mech. Engrg. 153 (1) (1998) 1–44.
[41] J.H. Chaudhry, J. Comer, A. Aksimentiev, L.N. Olson, A stabilized finite element method for modified Poisson–Nernst–Planck equations to determine ion flow through a nanopore, Commun. Comput. Phys. 15 (1) (2014) 93–125.
[42] H. Li, B.Z. Lu, An ionic concentration and size dependent dielectric permittivity Poisson–Boltzmann model for biomolecular solvation studies, J. Chem. Phys. 141 (2) (2014) 024115.
[43] L. Li, C. Li, Z. Zhang, E. Alexov, On the dielectric constant of proteins: smooth dielectric function for macromolecular modeling and its implementation in DelPhi, J. Chem. Theory Comput. 9 (4) (2013) 2126–2136.
[44] P. Kukic, D. Farrell, L.P. McIntosh, B. García-Moreno E, K.S. Jensen, Z. Toleikis, K. Teilum, J.E. Nielsen, Protein dielectric constants determined from NMR chemical shift perturbations, J. Am. Chem. Soc. 135 (45) (2013) 16968–16976.
[45] B.Z. Lu, Y.C. Zhou, Poisson–Nernst–Planck equations for simulating biomolecular diffusion–reaction processes II: size effects on ionic distributions and diffusion–reaction rates, Biophys. J. 100 (10) (2011) 2475–2485.
[46] S.Y. Bai, B.Z. Lu, VCMM: a visual tool for continuum molecular modeling, J. Mol. Graph. Model. 50 (2014) 44–49.
[47] L.P. Franca, S.L. Frey, T.J. Hughes, Stabilized finite element methods: I. Application to the advective–diffusive model, Comput. Methods Appl. Mech. Engrg. 95 (2) (1992) 253–276.
[48] T.J. Hughes, M. Mallet, M. Akira, A new finite element formulation for computational fluid dynamics: II. Beyond SUPG, Comput. Methods Appl. Mech. Engrg. 54 (3) (1986) 341–355.
[49] R. Codina, Comparison of some finite element methods for solving the diffusion–convection-reaction equation, Comput. Methods Appl. Mech. Engrg. 156 (1) (1998) 185–210.
[50] M. Bayrhuber, T. Meins, M. Habeck, S. Becker, K. Giller, S. Villinger, C. Vonrhein, C. Griesinger, Structure of the human voltage-dependent anion channel, Proc. Natl. Acad. Sci. USA 105 (40) (2008) 15370–15375.
[51] T.J. Dolinsky, J.E. Nielsen, J.A. McCammon, N.A. Baker, PDB2PQR: an automated pipeline for the setup, execution, and analysis of Poisson–Boltzmann electrostatics calculations, Nucleic Acids Res. 32 (2004) W665–W667.
[52] M. Chen, B.Z. Lu, TMSmesh: a robust method for molecular surface mesh generation using a trace technique, J. Chem. Theory Comput. 7 (1) (2011) 203–212.
[53] M.X. Chen, B. Tu, B.Z. Lu, Manifold meshing method preserving molecular surface topology, J. Mol. Graph. Model. 38 (2012) 411–418.
[54] C. Peter, G. Hummer, Ion transport through membrane-spanning nanopores studied by molecular dynamics simulations and continuum electrostatics calculations, Biophys. J. 89 (4) (2005) 2222–2234.
[55] J. Comer, A. Aksimentiev, Predicting the DNA sequence dependence of nanopore ion current using atomic-resolution Brownian dynamics, J. Phys. Chem. C 116 (5) (2012) 3376–3393.
[56] D. Gillespie, Energetics of divalent selectivity in a calcium channel: the ryanodine receptor case study, Biophys. J. 94 (2008) 1169–1184.
[57] J.C. Milne, R.J. Collier, pH-dependent permeabilization of the plasma membrane of mammalian cells by anthrax protective antigen, Mol. Microbiol. 10 (3) (1993) 647–653.
[58] J.C. Milne, D. Furlong, P.C. Hanna, J.S. Wall, R.J. Collier, Anthrax protective antigen forms oligomers during intoxication of mammalian cells, J. Biol. Chem. 269 (32) (1994) 20607–20612.
[59] T.L. Nguyen, Three-dimensional model of the pore form of anthrax protective antigen. Structure and biological implications, J. Biomol. Struct. Dyn. 22 (3) (2004) 253–265.
[60] V.A. Karginov, E.M. Nestorovich, M. Moayeri, S.H. Leppla, S.M. Bezrukov, Blocking anthrax lethal toxin at the protective antigen channel by using structure-inspired drug design, Proc. Natl. Acad. Sci. USA 102 (42) (2005) 15075–15080.